Solid Earth, 14, 1169–1179, 2023
https://doi.org/10.5194/se-14-1169-2023

Solid Earth Open Access EGU

The influence of extraction of various solvents on chemical properties on Chang 7 shale, Ordos Basin, China

Yan Cao[1,2], **Zhijun Jin**[1,2], **Rukai Zhu**[1,2,3], **and Kouqi Liu**[1,2]

[1]Institute of Energy, Peking University, Beijing 100871, China
[2]School of Earth and Space Sciences, Peking University, Beijing 100871, China
[3]Research Institute of Petroleum Exploration and Development, PetroChina, Beijing 100083, China

Correspondence: Zhijun Jin (jinzj1957@pku.edu.cn)

Received: 16 February 2023 – Discussion started: 30 March 2023
Revised: 30 July 2023 – Accepted: 27 September 2023 – Published: 7 November 2023

Abstract. To explore the effect of various solvents extraction on the chemical property of shale, several lacustrine shale samples from the Chang 7 member of the Upper Triassic Yanchang Formation, Ordos Basin, with maturities, from marginally mature ($T_{max} = 439°$) to late mature ($T_{max} = 456°$), were extracted by using acetone, tetrahydrofuran (THF), carbon disulfide (CS_2), and benzene, respectively. Fourier transform infrared spectroscopy (FTIR) was employed to examine the functional groups of the samples before and after extraction with different solvents. The results showed that the extraction yield from shale with THF is significantly higher than that of other solvents, which may be related to the properties of the THF, including the aromatic structure, high boiling point, excellent Hansen solubility parameters, and strong polarity. The total organic carbon (TOC)-normalized yield of the mature sample J1 is significantly higher than that of other samples, which may be related to the fact that the J1 sample is at the peak of hydrocarbon generation; thus, a large number of kerogens were cracked into oil and bitumen. The aromaticity of organic matter (OM) increases with the increase in the maturity. The length of the aliphatic chains of the OM first increased with the increase in the maturity before late maturity stage and then decreased in late maturity stage. The extraction of shale samples with solvents hardly changes the length of aliphatic chains. Higher aromaticity is observed in shale residues after THF extractions than for other solvents (i.e., acetone, CS_2, and benzene).

1 Introduction

Due to the increasingly serious energy shortage problems associated with the exhaustion of fuel energy resources, potential unconventional fossil sources are highly desired (Yang et al., 2019; Li et al., 2022). The quest to produce unconventional petroleum-based fuels and achieve energy independence is being aggressively pursued in China and the United States (Overland, 2015). In the past few years, shale oil has been regarded as an important resource that can be exploited commercially due to the technical innovations of three-dimensional development in horizontal wells and fracture-controlled fracking (Li et al., 2020; S. Zhou et al., 2020; Lei et al., 2021; H. Yang et al., 2021). For China, the government has been encouraging shale oil developments to address the shortage of domestic oil resources and the rising energy demand and to safeguard the country's long-term energy security (Yang et al., 2019; Hu et al., 2020; L. Zhou et al., 2020; Lu et al., 2022).

Extraction has become a common shale pretreatment method in the laboratory to study the pore structures related to organic matter (OM; Qi et al., 2019; Wang et al., 2020; S. Yang et al., 2021). However, different solvents could affect shale extraction efficiency and methane adsorption capacity (Cao et al., 2019, 2020). For the shale samples, the extraction by using acetone, CS_2, and benzene can be used to reveal the micropores, mesopores, and macropores, respectively (Cao et al., 2019). In addition, during the development of shale oil, the chemical properties of shale after being extracted by using different organic solvents are also different (Cao et al., 2020). Wei et al. (2014) found that the hydrocar-

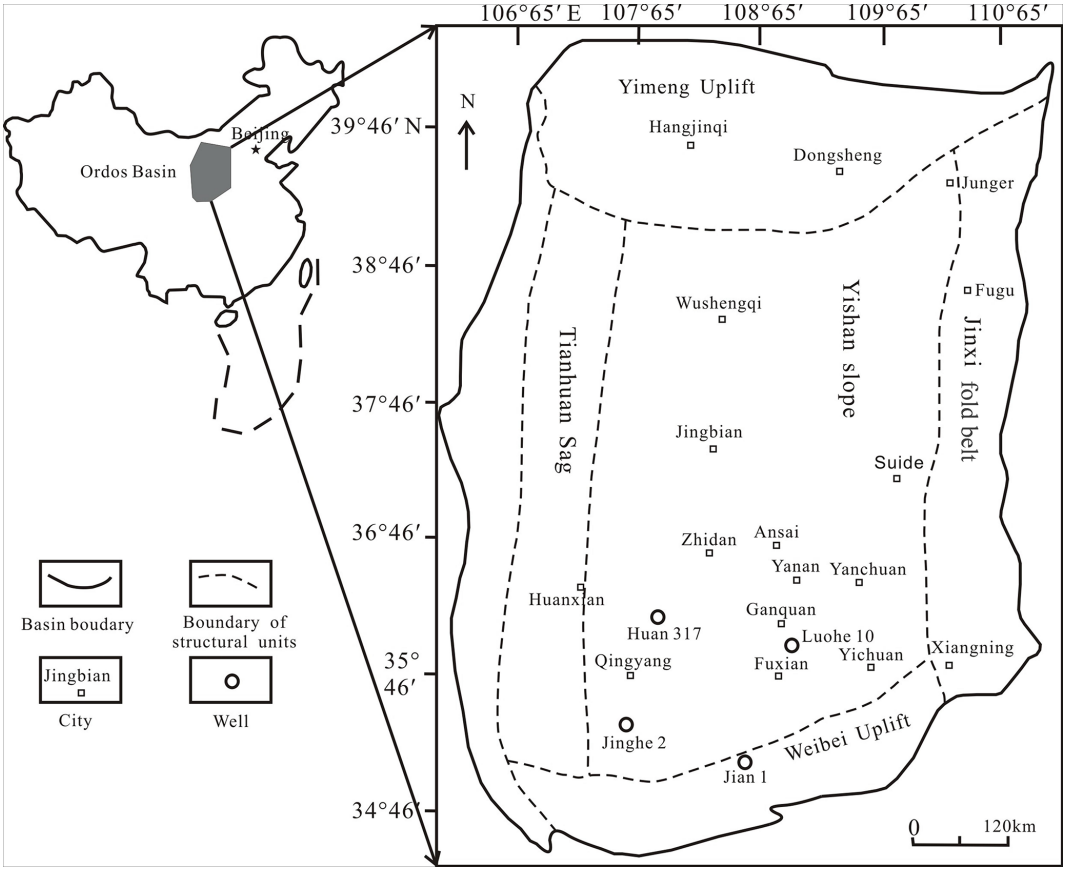

Figure 1. Locations of sampling wells and simplified structural framework across the Ordos Basin (modified from Cao et al., 2019).

bons in toluene extract exhibit remarkable aromaticity. Furmann et al. (2013) showed that the organic aromaticity of extractions from dichloromethane is greater than that from methanol.

A large number of studies focus on either the changes in shale pore structure before and after extraction (Gorynski et al., 2019; Qi et al., 2019; H. and S. Yang et al., 2021) or the functional groups of OM extracted from underground fossil energy (Chen et al., 2012; Mastalerz et al., 2012; Furmann et al., 2013; Wei et al., 2014). In fact, underground shale is often washed out of OM by organic solvent extraction in the laboratory to explore the relationship between OM and an inorganic mineral skeleton in shale. It is worth mentioning that this study is a continuation of our earlier published study, which details the findings about influence of extraction on shale pore structure with different maturity using various solvents (Cao et al., 2019, 2020). However, the study of the changes in the chemical properties in the lacustrine organic-rich shale of different maturity before and after extraction with different solvents is rarely reported. Our results of the study will help in the selection of organic solvents for oil-washing experiments in shale samples of different maturity.

Fourier transform infrared spectroscopy (FTIR) is an advanced method for the determination of chemical structures (e.g., functional groups) of OM (Wei et al., 2014). In this study, several lacustrine shale samples with different maturities from Chang 7 member of the Upper Triassic Yanchang Formation, Ordos Basin, central China, were collected. The present study is a continuation of our previous research (Cao et al., 2019, 2020); Soxhlet extractions with four different solvents (tetrahydrofuran, carbon disulfide, benzene, and acetone) were performed on the selected shale samples. Interestingly, the Fourier transform infrared spectroscopy (FTIR) was performed on the samples before and after the extraction. After that, the influence of various solvent extraction on chemical properties in lacustrine shale of different maturity was summarized.

2 Geological settings and samples

According to the basement and faults, the Ordos Basin is divided into six secondary structural units, namely the Weibei uplift, the Yishan slope, the Tianhuan depression, the Yimeng uplift, the western margin thrust belt, and Jinxi flexural fold belt (Fig. 1; Guo et al., 2014). The Yishan slope is inclined to the west, with a slope of about 1° (Guo et al., 2014). The Chang 7 member was developed during the largest lacustrine

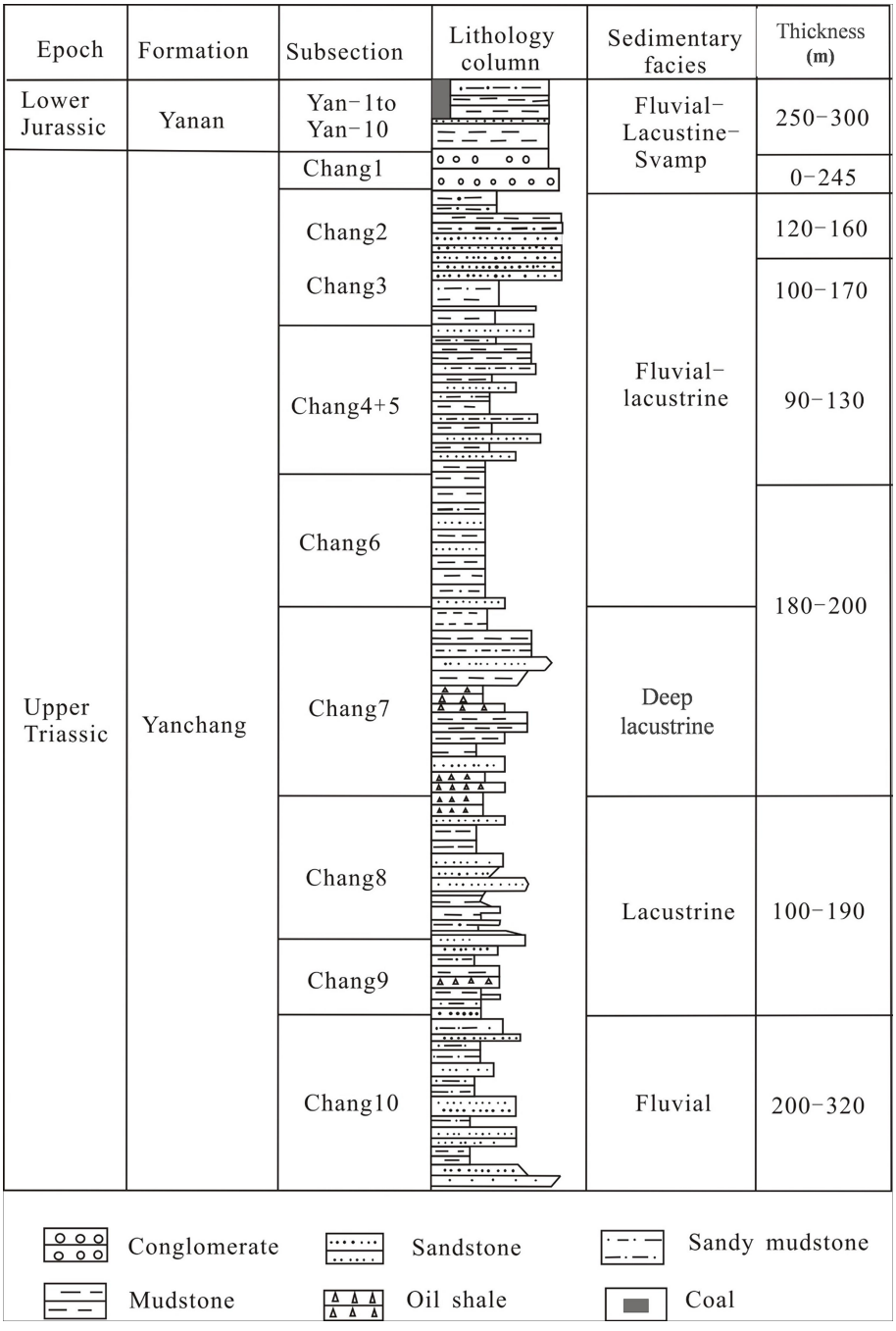

Figure 2. The strata and sedimentary characteristics of the Yanchang Formation of the Upper Triassic (modified from Cao et al., 2020).

flooding in the lake basin (Fig. 1; Guo et al., 2014). Yellowish tuff intervals are interbedded within the Yanchang sediments ranging from 0.2 to 0.45 cm (0.08–0.18 in.; Qiu et al., 2014). The Yanchang Formation of the Upper Triassic can be divided into 10 sub-segments (i.e., Chang 1–10; Fig. 2). The Chang 7 member is mainly made up of silty mudstone and shale samples and has great potential for shale oil or gas (Fig. 2; Duan et al., 2008; Lei et al., 2015). The Chang 7 member shale develops a large area of high-quality source rocks (about 5×10^4 km^2), which is rich in oil-prone OM derived from acritarchs (*Leiosphaeridia* species) and some *Botryococcus* (Ji et al., 2010). The cumulative thickness is mostly between 10 and 50 m, and the maximum thickness can reach more than 80 m (Guo et al., 2014). In this paper, several shale samples with different maturities in Chang 7 member of the Upper Triassic Yanchang Formation were obtained from the wells of Huan 317, Jian 1, Luohe 10, and Jinghe 2, respectively (Fig. 1). The samples selected for this

study have been analyzed in our previous publications (Cao et al., 2020).

3 Experiments

3.1 Geochemical analysis

The samples were crushed to 180–200 mesh prior to geochemical analysis. The total organic carbon (TOC) content was tested by a LECO CS-344 carbon and sulfur analyzer. The type, maturity, and hydrocarbon generation potential of OM were determined. The temperature at which the most S_2 is generated is regarded as the maximum pyrolysis yield temperature (T_{max}; °C), and the hydrogen index (HI; mg HC/g TOC) was obtained from the ratio of S_2 to TOC (Peters, 1986).

3.2 X-ray diffraction

The samples were tested by a D/Max 2500 diffractometer, and the tests follow two separate processes of the CPSC procedure (CPSC, 2010). The actual mineral content of the samples was obtained by quantitative X-ray diffraction (XRD) analysis of samples smaller than 200 mesh (< 0.075 mm).

3.3 Soxhlet extraction

The bulk shale samples were uniformly crushed into 60 mesh with a laboratory knife mill and then evenly divided into five parts. The sample was extracted using solvents of different aromaticity, polarity, and permeability, namely acetone, tetrahydrofuran, carbon disulfide, and benzene; the remaining original sample was used as a control. About 1000 g solvent and 50 g shale sample were sealed in a Soxhlet extractor to prevent solvent loss. The extraction time lasted 150 h until the solvent became colorless. Samples were named according to their corresponding abbreviated well names (JH2, J1, LH10, and H317; Table 2), and the original shale samples were marked by the shorthand subscript, following the sample name ($JH2_{orig}$, $J1_{orig}$, $LH10_{orig}$, and $H317_{orig}$). The residue (e.g., JH2) from tetrahydrofuran (THF), acetone, CS_2, and benzene extraction was clearly characterized by $JH2_T$, $JH2_A$, $JH2_C$, and $JH2_B$, respectively.

3.4 Potassium bromide (KBr) and FTIR analysis

Both powdered original shale samples and their corresponding extracted shale residues (∼ 2 mg) were blended with potassium bromide (KBr; ∼ 200 mg) and pressed into pellets. Through the use of a Nicolet 6700 FT-IR spectrometer collecting 200 scans per sample at a resolution of 4 cm^{-1}, the vibration frequencies of specific atomic bonds were analyzed. Thus, the chemical functional groups could be assessed using a standard semi-quantitative technique. For the KBr–FTIR characterization, each spectrum was recorded in the spectral range of 400–3250 cm^{-1}. The bands of absorption were identified by comparing the spectrums with published studies (Drobniak and Mastalerz, 2006; Furmann et al., 2013).

According to a manual mode, the band area was determined using Origin software. These integrated band areas were used to calculate ratios for the (1) aromaticity, including $AR1 = [(\delta ArC=C/\nu AlC\text{-}H) + \delta ArC=C]$, $AR2 = (\nu ArC\text{-}H/\nu AlC\text{-}H)$, and $AR3 = (\gamma ArC\text{-}H/\nu AlC\text{-}H)$; (2) length of aliphatic chains, namely $LAC = (CH_2/CH_3)$ in νAlC-H; and (3) degree of substitution (DOS) of aromatic sites by alkyl groups, namely $DOS = (\gamma ArC\text{-}H(1\ adjacent\ H)/\gamma ArC\text{-}H$ (4 adjacent H); Wei et al., 2014). The detailed definitions of the parameters can be found in Tables 1 and 4.

The representative spectrums of the original shale samples and corresponding residues are presented in Figs. 5 and 6, respectively. In terms of the length of aliphatic chains (LAC), longer n-alkyl chains are determined by CH_2 bands, whereas shorter n-alkyl and branched aliphatic chains are indicated by CH_3 bands (Table 4). The DOS of aromatic rings represents the fraction of aromatic sites where hydrogen atoms are substituted by alkyl groups (Table 4).

4 Results

4.1 Geochemical characteristics

The geochemical features of shale samples are listed in Table 2. Four selected samples span from marginally mature (JH2; 439 °C) to late mature (H317; 460 °C), based on the Chinese continental hydrocarbon source rock geochemical evaluation method (SY/T 5735-1995, 1995). The kerogen type of selected samples is type I or II_1 (Fig. 3; Tong et al., 2011). TOC content is generally high, ranging from 3.79 wt % to 22.19 wt % (Table 2). The hydrocarbon generation potential ($S_1 + S_2$) ranges from 8.11 to 127.42 mg g^{-1}. Table 2 shows that the hydrogen index (HI) of the samples is in the range of 155–528 mg g^{-1}.

4.2 Mineral compositions

The samples contain a large number of clay minerals (42.8 wt %–54.2 wt %, with an average of 48.15 %). An illite–smectite mixed layer or illite are the most dominant clay types (Table 3). In general, the content of the felsic component is between 19.5 wt % and 52.2 wt %, with the average of 40.63 %. In addition, the pyrite content of the studied samples varies greatly, ranging from 0.9 wt % to 25.5 wt % (Table 3).

4.3 Extraction yields

The extraction data of the studied samples with different solvents are shown in Fig. 4. Among all the solvents, THF has the highest extraction efficiency (2.44 wt %–4.43 wt %;

Table 1. Fourier transform infrared (FTIR) bands used in this study (Chen et al., 2012).

FTIR band	For marginally mature shale samples JH2 T_{max}; (439°) wave numbers (cm^{-1})	For mature shale samples J1 T_{max}; (449°) wave numbers (cm^{-1})	For late mature shale LH10 T_{max}; (454°) wave numbers (cm^{-1})	For late mature shale H317 T_{max}; (456°) wave numbers (cm^{-1})
νArC-H	3046–2992	3062–2992	3084–3005	3062–3000
ν Al C-H	2970–2812	2970–2809	2983–2809	2984–2814
$\nu_{as}CH_3$	2970–2874	2970–2877	2970–2887	2984–2882
ν_sCH_2	2874–2812	2877–2809	2887–2798	2882–2814
δArC = C	1705–1575	1701–1561	1719–1552	1707–1552
δAlC-H	1484–1386	1477–1400	1487–1389	1482–1381
γArC-H	945–667	946–673	939–673	948–673
γArC-H 1	945–833	930–886	940–812	948–817
γArC-H 2	833–721	814–707	812–709	817–707
γArC-H 4	721–667	707–673	709–673	707–673

Ar is for aromatic; Al is for aliphatic; ν is for stretching vibration; δ is for deformation vibration in plane; γ is for deformation vibration out of plane; as is for asymmetric; and s is for symmetric.

Table 2. Geochemical features of the original shale samples and the corresponding residues.

Sample	S_1 ($mg\,g^{-1}$)	S_2 ($mg\,g^{-1}$)	T_{max} (°C)	TOC (%)	OM type	HI ($mg\,g^{-1}$)	Maturity stage
JH2	10.19	117.23	439	22.19	I	528	Marginally mature
J1	2.23	5.88	449	3.79	II_1	155	Mature
LH10	11.31	47.42	454	16.23	I	292	Late mature
H317	5.39	33.89	456	18.03	I	188	Late mature

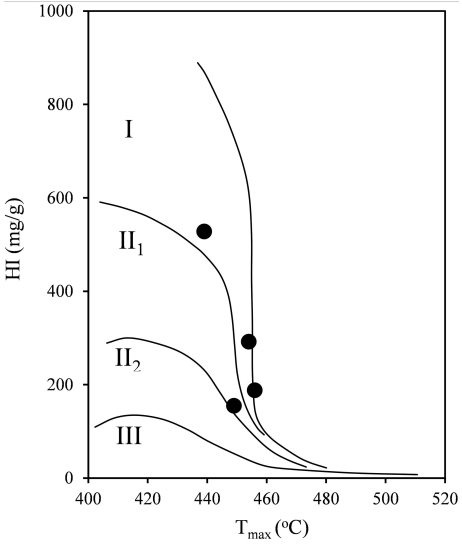

Figure 3. Plot of HI versus T_{max} for the original shale samples (based on Espitalie et al., 1985).

Fig. 4a). According to the TOC-normalized yield of extracts, the mature samples J1 ($T_{max} + 449°$) had significantly higher extractable samples (13.48 wt %–56.91 wt %) than other samples ($\leq$ 5.28 wt %; Fig. 4b).

4.4 FTIR spectroscopy

The representative spectrums of the original shale samples and corresponding residues are presented in Figs. 5 and 6, respectively. The FTIR results after extraction are summarized in Table 4. The OM in shale is a three-dimensional macromolecule composed of aromatic clusters and aliphatic chains (Tong et al., 2011; Guan et al., 2015; Wang et al., 2016, 2017; Zhao et al., 2018). The aromaticity (i.e., AR2 and AR3) of the samples follows the order H317 (3.327) > LH10 (3.225) > J1 (3.038) > JH2 (2.828; Table 4), which is consistent with maturity. In addition, shale residues from THF extraction possess higher aromaticity than those from other solvents. Unlike aromaticity, the length of aliphatic chains (LAC) does not increase monotonically with the increase in the maturity (Table 4). However, there is no regularity in the DOS (i.e., the fraction of aromatic sites where hydrogen atoms are substituted by alkyl groups) of different maturity shale samples, and the DOS of shale be-

Table 3. Mineral compositions of the studied samples.

Sample	Quartz (wt %)	Feldspar (wt %)	Pyrite (wt %)	Gypsum (wt %)	All clays (wt %)	Illite/ smectite (wt %)	Illite (wt %)	Kaolinite (wt %)	Chlorite (wt %)	Mixed-layer ratio (I/S) S; %
JH2	12	7.5	25.5	0.8	54.2	70	9	21	Unitless	19
J1	36.5	12.7	0.9	Unitless	49.9	62	18	8	12	18
LH10	23.2	29	2.1	Unitless	45.7	66	15	7	12	11
H317	29.7	11.9	15.6	Unitless	42.8	2	88	2	8	24

Unitless indicates that the content of individual mineral was not determined.

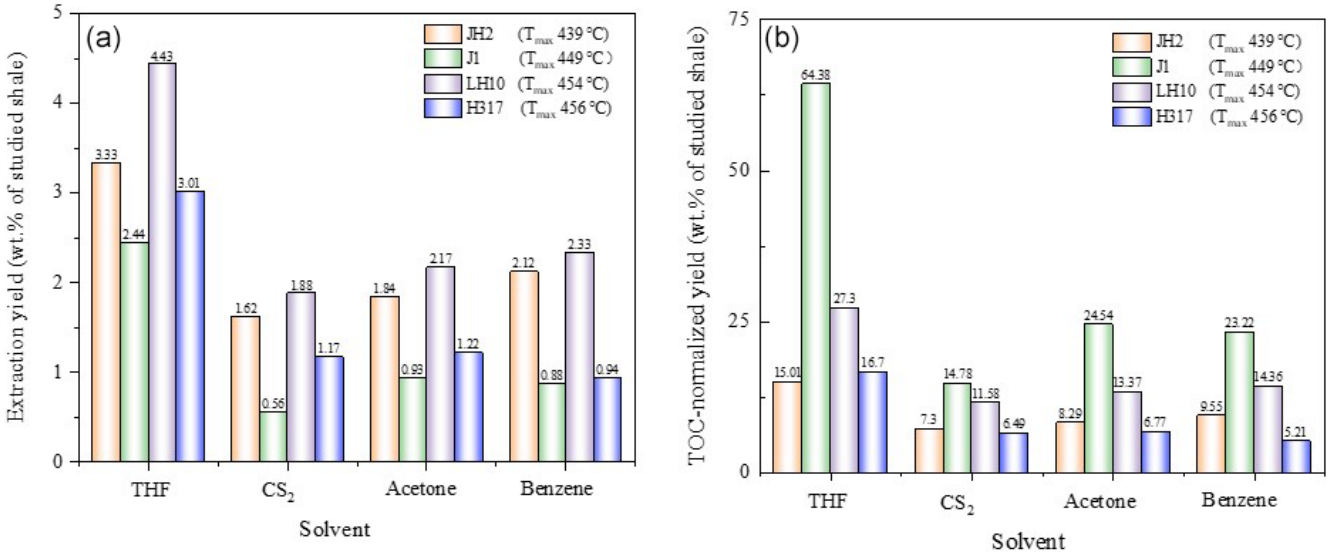

Figure 4. Extraction data of the studied samples with solvents of acetone, THF, benzene, and CS_2. **(a)** Original extraction yield and **(b)** TOC-normalized yield of extracts.

fore and after extraction with different solvents demonstrated an irregular change (Table 4).

5 Discussion

5.1 The influence of solvents on extraction yield and composition of the soluble mixture

Previous studies have found that the extraction yields of shale and the composition of the soluble mixture are related to the properties of the solvent, extraction temperature, the geochemical parameters of the shale, and so on (Hu et al., 1999; Olukcu et al., 1999; Shaohui et al., 2000; Abourriche et al., 2013; Cao et al., 2019). As the polarity of the solvent increases, the extraction yield increases accordingly (Masaki et al., 2004). The solvent dissolution capacity has obvious temperature dependence, and the dissolution capacity increases with the increase in the temperature (Hu et al., 1999). The increase in extraction pressure and temperature will promote the activation energy of the sample (Allawzi et al., 2011).

The Hansen solubility parameters of the four solvents are shown in Table 5; the extraction ability of CS_2 is similar to that of benzene (Table 5). Because of the aromatic structure, high boiling point, and strong polarity, THF could have a stronger extraction ability than other solvents (Table 5).

Allawzi et al. (2011) found that the OM obtained by solvent extraction is mainly composed of low molecular weight compounds (e.g., saturated hydrocarbons, olefin hydrogen, and aromatic compounds). Our results show that the extraction yield of shale with THF is significantly higher than that of other solvents (Fig. 4a), which could be attributed to the fact that a mass of the heaviest macromolecular compound of asphaltene was screened out (Cao et al., 2020). The significant elimination of OM (i.e., asphaltene) by THF may be related to the properties of the THF, including the aromatic structure (Johnson et al., 1967), high boiling point (Cao et al., 2019), excellent Hansen solubility parameters, and strong polarity (Toolan et al., 2016; Table 5), which could assist to destroy the interact between shale matrix and the asphaltenes (i.e., a complex molecular architecture with a central poly-

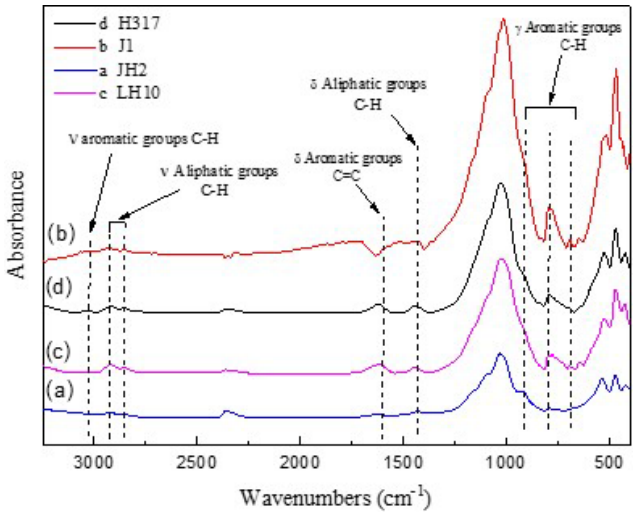

Figure 5. FTIR spectra of original **(a)** marginally mature sample $JH2_{orig}$ ($T_{max} = 439\,°C$), **(b)** the mature sample $J1_{orig}$ ($T_{max} = 449\,°C$), **(c)** late mature sample $LH10_{orig}$ ($T_{max} = 454\,°C$), and **(d)** late mature sample $H317_{orig}$ ($T_{max} = 456\,°C$).

cyclic aromatic hydrocarbon (PAH), with peripheral alkane substituents; Schuler et al., 2017) of PAH molecular polymerization (Schuler et al., 2015).

The extraction yields of the studied samples are of the order of LH10, JH2, H317, and J1, regardless of solvents (Fig. 4a), which may be due to the soluble hydrocarbon content (S_1) of the studied sample (Table 2). According to the TOC-normalized yield of extracts, the mature samples J1 ($T_{max} = 449°$) had significantly higher extractable samples than other samples (Fig. 4b), which may be related to the fact that the J1 sample ($T_{max} = 449°$) was at the peak of hydrocarbon generation. Thus, a large number of kerogens were cracked into oil and bitumen (Ertas et al., 2006; Wei et al., 2014). However, a little kerogen was converted to a small amount of oil in the early maturity stage (Cao et al., 2020), so the TOC-normalized extraction yield of the JH2 sample is low. However, the TOC-normalized extraction yield of late mature shale H317 is similar to that of early mature shale JH2, which could be attributed to the fact that some of the oil is cracked to natural gas or transported to other locations with maturation (Cao et al., 2020).

5.2 Effect of solvent extraction on the chemical structure of shale samples

The application of FTIR spectroscopy provides an evaluation of the aromaticity and length of aliphatic chains for original shale samples and residues from extractions. Table 4 showed that the aromaticity (AR2 and AR3) of the original shale OM with different maturity is obviously different and ranges from 2.828 to 3.327. Figure 7 shows there is a positive correlation between aromaticity and maturity in shale (Feng et al., 2013). Thus, the abovementioned facts indicate that the thermal maturation can increase the aromaticity of shale OM.

Table 4. FTIR results from original shale and extracted shale residues.

	FTIR absorbance ratios[a]				
	AR1[b]	AR2	AR3	LAC	DOS
Shale residues after extraction JH2 shale					
Original shale	2.352	0.010	2.818	0.242	11.498
After extraction with					
Acetone	0.000	0.039	2.156	0.288	8.935
CS_2	0.000	0.092	2.449	0.269	6.861
Benzene	4.996	0.004	2.412	0.252	9.382
THF	5.114	0.024	2.893	0.262	10.494
J1 shale					
Original shale	6.399	0.064	2.974	0.257	1.700
After extraction with					
Acetone	6.731	0.011	20.006	0.232	1.654
CS_2	9.573	0.172	16.903	0.308	1.997
Benzene	5.063	0.012	18.416	0.237	2.012
THF	0.000	0.253	22.122	0.335	1.492
LH10 shale					
Original shale	7.167	0.103	3.122	0.298	2.897
After extraction with					
Acetone	10.632	0.101	3.500	0.270	2.655
CS_2	8.381	0.092	3.371	0.268	2.933
Benzene	2.466	0.228	3.000	0.352	2.859
THF	7.667	0.119	4.041	0.289	2.780
H317 shale					
Original shale	8.347	0.068	3.259	0.272	1.686
After extraction with					
Acetone	0.000	0.627	2.844	0.858	2.181
CS_2	5.472	0.066	3.749	0.243	2.129
Benzene	0.000	0.268	2.313	0.485	2.031
THF	0.000	0.3420	3.753	0.551	1.624

[a] The integrated peak areas were used to calculate FTIR ratios. [b] AR1 = 0 for residues because aromatic bands (δArC = C, νArC-H) were not present in the FTIR spectrum.

Table 4 showed that the length of aliphatic chains (LAC) from late mature shale (i.e., LH10 and H317) is higher than those of mature shale J1 and marginally mature shale JH2. In addition, the LAC of the early mature shale J1 is also higher than the marginally mature shale JH2 (Table 4). However, the LAC of the higher-maturity H317 shale ($T_{max} = 456°$) is lower than that of mature LH10 shale ($T_{max} = 454°$). Those values indicate that the aliphatic chains lengthened with the increase in the maturity before the late maturity stage (Feng

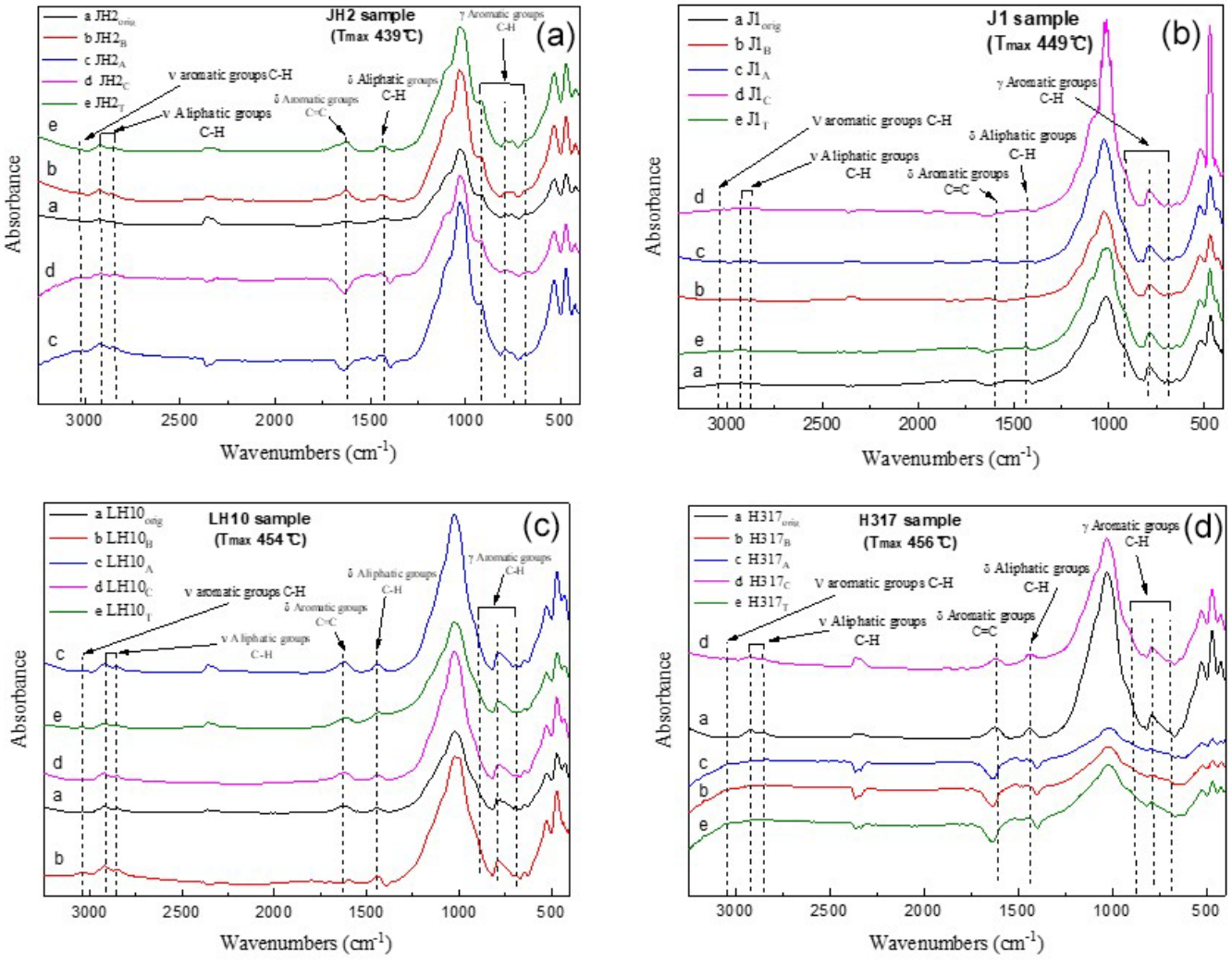

Figure 6. A comparison of FTIR spectra of original samples and residues.

Table 5. The properties of the four solvents (Cao et al., 2020).

Solvent	Hansen solubility parameters			Polarity	Boiling point	Aromaticity
	Dispersion	Polarity	H bond			
THF	16.8	5.7	8	4.2	65 °C	Aromatic
CS_2	20.2	0	0.6	0.15	46.5 °C	Non-aromatic
Acetone	15.5	10.4	7	5.4	56 °C	Non-aromatic
Benzene	18.4	0	2	3	80 °C	Aromatic

et al., 2013) and then shortened as the maturity further increases. That may be attributed to the fact that kerogen cracking to form a large amount of bitumen at the low-maturity stage leads to longer aliphatic chains with increasing maturity, while at the high-maturity stage, bitumen is largely consumed, and the OM represented by bitumen is further cracked, thus shortening the aliphatic chains with increasing maturity (Feng et al., 2013). However, previous studies have also observed that aliphatic chains lengthened become monotonically shorter and/or more branched with maturity, which indicates that longer aliphatic chains can be preferentially cleaved. The cleavage of the C–C bonds between carbons α and β to a ring could explain this result (Lin and Ritz, 1993). Moreover, the large differences in the sources of OM in different regions may be the cause of the above contradictions.

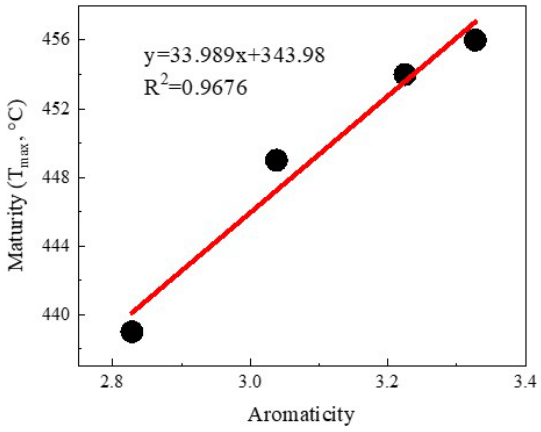

Figure 7. Relationships between the aromaticity and the maturity in shale OM.

The DOS of aromatic rings represents the fraction of aromatic sites, where hydrogen atoms are substituted by alkyl groups, and there is no regularity in the DOS (i.e., the fraction of aromatic sites where hydrogen atoms are substituted by alkyl groups) of different maturity shale samples (Table 4). Therefore, the fraction of aromatic sites where hydrogen atoms are substituted by alkyl groups in shale is independent of maturity.

In addition, the FTIR-derived LAC values smaller than 1 show the superiority of CH_3 bands (i.e., asymmetric stretching vibration) in shale samples corresponding to short and branched aliphatic chains (Furmann et al., 2013). Our results demonstrate that aliphatic chains are shorter with higher branching in the original shale samples, which could not be changed during the extractions (Table 4). In addition, the FTIR of shale samples after different solvent extractions is irregular, which may be influenced by the inorganic minerals. Therefore, it seems much more reasonable to conclude that FTIR was unable to detect any significant change in the LAC values due to solvent extraction. Furthermore, the aromaticity (both AR2 and AR3) of residues after THF extractions is significantly higher than those after the extraction of other solvents (Table 4), which may be related to the fact that THF only dissolves relatively fewer aromatic hydrocarbons from shale samples (Cao et al., 2020), and the residual abundant aromatic hydrocarbons in shale benefits OM aromaticity (Monger, 1984).

6 Conclusions

Soxhlet extractions with THF, benzene, CS_2, and acetone, respectively, have been applied to the shale samples with a progressive maturation gradient in order to gain insights into the proportion of soluble hydrocarbon and the chemical characteristics of shale with different maturity. The following conclusions have been obtained.

1. The extraction yield of shale with THF is significantly higher than that of other solvents, which may be related to the properties of the THF, including the aromatic structure, high boiling point, excellent Hansen solubility parameters, and strong polarity. The TOC-normalized yield of the mature sample J1 is significantly higher than that of other samples, which may be related to that the J1 sample is at the peak of hydrocarbon generation; thus, a large number of kerogens were cracked into oil and bitumen.

2. Thermal maturation of shale samples can increase the aromaticity of OM. The aliphatic chains in the shale OM lengthened with the increase in the maturity before the late maturity stage, and then shortened with the further increase in the maturity in the late maturity stage.

3. The extraction of shale samples with solvents hardly changes the length of aliphatic chains. Higher aromaticity is observed in shale residues after THF extractions than other solvents (i.e., acetone, CS_2, and benzene).

Data availability. Data will be made available on request to the corresponding author.

Author contributions. YC was responsible for the conceptualization and methodology of the study, carrying out the experiments, compiling and analyzing the data, and writing the paper. ZJ was responsible for the acquisition and management of financial support and contribution to experimental design. RZ and KL investigated and revised the ideas of the article. All authors contributed to the review of the paper.

Competing interests. The contact author has declared that none of the authors has any competing interests.

Disclaimer. Publisher's note: Copernicus Publications remains neutral with regard to jurisdictional claims made in the text, published maps, institutional affiliations, or any other geographical representation in this paper. While Copernicus Publications makes every effort to include appropriate place names, the final responsibility lies with the authors.

Acknowledgements. Our research partners, Hui Han and Chen Guo of Southwest Petroleum University, made substantial contributions to the FTIR experiments, for which we are sincerely grateful.

Financial support. This study was jointly funded by the National Science Foundation of China (grant no. 42090025) and the 2022 American Association of Petroleum Geologists Foundation Grants-in-Aid program (Grants-in-Aid general fund grant).

Review statement. This paper was edited by Andrea Di Muro and reviewed by two anonymous referees.

References

Abourriche, A. K., Oumam, M., Hannache, H., Birot, M., Abouliatim, Y., Benhammou, A., El Hafiane, Y., Abourriche, A. M., Pailler, R., and Naslain, R.: Comparative studies on the yield and quality of oils extracted from Moroccan oil shale, J. Supercrit. Fluids, 84, 98–104, https://doi.org/10.1016/j.supflu.2013.09.018, 2013.

Allawzi, M., Al-Otoom, A., Allaboun, H., Ajlouni, A., and Al Nseirat, F.: CO_2 supercritical fluid extraction of Jordanian oil shale utilizing different co-solvents, Fuel Process. Technol., 92, 2016–2023, https://doi.org/10.1016/j.fuproc.2011.06.001, 2011.

Cao, Y., Han, H., Liu, H. W., Jia, J. C., Zhang, W., Liu, P. W., Ding, Z. G., Chen, S. J., Lu, J. G., and Gao, Y.: Influence of solvents on pore structure and methane adsorption capacity of lacustrine shales: An example from a Chang 7 shale sample in the Ordos Basin, China, J. Petrol. Sci. Eng., 178, 419–428, https://doi.org/10.1016/j.petrol.2019.03.052, 2019.

Cao, Y., Han, H., Guo, C., Pang, P., Ding, Z. G., and Gao, Y.: Influence of extractable organic matters on pore structure and its evolution of Chang 7 member shales in the Ordos Basin, China: Implications from extractions using various solvents, J. Nat. Gas Sci. Eng., 79, 103370, https://doi.org/10.1016/j.jngse.2020.103370, 2020.

Chen, Y., Mastalerz, M., and Schimmelmann, A.: Characterization of chemical functional groups in macerals across different coal ranks via micro-FTIR spectroscopy, Int. J. Coal Geol., 104, 22–33, https://doi.org/10.1016/j.coal.2012.09.001, 2012.

CPSC – China Petroleum Standardization Committee: Analysis Method for Clay Minerals and Ordinary Non-clay Minerals in Sedimentary Rocks by X-Ray Diffraction, SY/T 5163-2010, https://www.gb-gbt.cn/PDF.aspx/SYT5163-2010.2010.10.01 (last access: 6 November 2023), 2010.

Drobniak, A. and Mastalerz, M.: Chemical evolution of Miocene wood: Example from the Belchatow brown coal deposit, central Poland, Int. J. Coal Geol., 66, 157–178, https://doi.org/10.1016/j.coal.2005.06.004, 2006.

Duan, Y., Wang, C. Y., Zheng, C. Y., Wu, B. X., and Zheng, G. D.: Geochemical study of crude oils from the Xifeng oilfield of the Ordos basin, China, J. Asian Earth Sci., 31, 341–356, https://doi.org/10.1016/j.jseaes.2007.05.003, 2008.

Ertas, D., Kelemen, S. R., and Halsey, T. C.: Petroleum expulsion part 1. Theory of kerogen swelling in multicomponent solvents, Energy Fuels, 20, 295–300, https://doi.org/10.1021/ef058024k, 2006.

Espitalie, J., Deroo, G., and Marquis, F.: Rock-Eval pyrolysis and its applications (part 2), Rev. Inst. Fr. Pet., 40, 755–784, 1985.

Feng, Y., Van Le Doan, T., and Pomerantz, A. E.: The chemical composition of bitumen in pyrolyzed green river oil shale: Characterization by ^{13}C NMR spectroscopy, Energy Fuels, 27, 7314–7323, https://doi.org/10.1021/ef4016685, 2013.

Furmann, A., Mastalerz, M., Brassell, S. C., Schimmelmann, A., and Picardal, F.: Extractability of biomarkers from high- and low-vitrinite coals and its effect on the porosity of coal, Int. J. Coal Geol., 107, 141–151, https://doi.org/10.1016/j.coal.2012.09.010, 2013.

Gorynski, K. E., Tobey, M. H., Enriquez, D. A., Smagala, T. M., Dreger, J. L., and Newhart, R. E.: Quantification and characterization of hydrocarbon-filled porosity in oil-rich shales using integrated thermal extraction, pyrolysis, and solvent extraction, Am. Assoc. Petrol. Geol. Bull., 103, 723–744, https://doi.org/10.1306/08161817214, 2019.

Guan, X. H., Liu, Y., Wang, D., Wang, Q., Chi, M. S., Liu, S., and Liu, C. G.: Three-Dimensional Structure of a Huadian Oil Shale Kerogen Model: An Experimental and Theoretical Study, Energy Fuels, 29, 4122–4136, https://doi.org/10.1021/ef502759q, 2015.

Guo, H., Jia, W., Peng, P., Lei, Y., Luo, X., Cheng, M., Wang, X., Zhang, L., and Jiang, C.: The composition and its impact on the methane sorption of lacustrine shales from the Upper Triassic Yanchang Formation, Ordos Basin, China, Mar. Petrol. Geol., 57, 509–520, https://doi.org/10.1016/j.marpetgeo.2014.05.010, 2014.

Hu, H., Zhang, J., Guo, S., and Chen, G.: Extraction of Huadian oil shale with water in sub- and supercritical states, Fuel, 78, 645–651, https://doi.org/10.1016/S0016-2361(98)00199-9, 1999.

Hu, S., Zhao, W., Hou, L., Yang, Z., Zhu, R., Wu, S., Bai, B., and Jin, X.: Development potential and technical strategy of continental shale oil in China, Petrol. Explor. Dev., 47, 877–887, https://doi.org/10.1016/S1876-3804(20)60103-3, 2020.

Ji, L. ming, Yan, K., Meng, F. W., and Zhao, M.: The oleaginous Botryococcus from the Triassic Yanchang Formation in Ordos Basin, Northwestern China: Morphology and its paleoenvironmental significance, J. Asian Earth Sci., 38, 175–185, https://doi.org/10.1016/j.jseaes.2009.12.010, 2010.

Johnson, R. N., Farnham, A. G., Clendinning, R. A., Hale, W. F., and Merriam, C. N.: Poly(aryl ethers) by nucleophilic aromatic substitution. I. Synthesis and properties, J. Polym. Sci. Pt. A, 5, 2375–2398, https://doi.org/10.1002/pol.1967.150050916, 1967.

Lei, Q., Weng, D., Xiong, S., Liu, H., Guan, B., Deng, Q., Yan, X., Liang, H., and Ma, Z.: Progress and development directions of shale oil reservoir stimulation technology of China National Petroleum Corporation, Petrol. Explor. Dev., 48, 1198–1207, https://doi.org/10.1016/S1876-3804(21)60102-7, 2021.

Lei, Y., Luo, X., Wang, X., Zhang, L., Jiang, C., Yang, W., Yu, Y., Cheng, M., and Zhang, L.: Characteristics of silty laminae in Zhangjiatan shale of southeastern Ordos Basin, China: Implications for shale gas formation, Am. Assoc. Petrol. Geol. Bull., 99, 661–687, https://doi.org/10.1306/09301414059, 2015.

Li, Y., Chen, S., Wang, Y., Su, K., He, Q., Qiu, W., and Xiao, Z.: Relationships between hydrocarbon evolution and the geochemistry of solid bitumen in the Guanwushan Formation, NW Sichuan Basin, Mar. Petrol. Geol., 111, 116–134, https://doi.org/10.1016/j.marpetgeo.2019.08.018, 2020.

Li, Y., Lu, J., Liu, X., Wang, J., Ma, W., He, X., Mou, F., and Li, X.: Geochemistry and origins of natural gas in the Hong-Che fault zone of the Junggar Basin, NW China, J. Petrol. Sci. Eng., 214, 110501, https://doi.org/10.1016/j.petrol.2022.110501, 2022.

Lin, R. and Patrick Ritz, G.: Studying individual macerals using i.r. microspectrometry, and implications on oil versus gas/condensate proneness and "low-rank" generation, Org. Geochem., 20, 695–706, https://doi.org/10.1016/0146-6380(93)90055-G, 1993.

Lu, J., Liao, J., Liu, X., Li, Y., Yao, J., He, Q., Xiao, Z., He, X., Fu, X., and Li, X.: Geochemistry of different source rocks and oil-source correlation of lacustrine sedimentary successions: A case study of the Triassic Yanchang formation in the Dingbian-Wuqi Area, Ordos Basin, Northern China, J. Asian Earth Sci., 232, 105216, https://doi.org/10.1016/j.jseaes.2022.105216, 2022.

Masaki, K., Yoshida, T., Li, C., Takanohashi, T., and Saito, I.: The effects of pretreatment and the addition of polar compounds on the production of "HyperCoal" from subbituminous coals, Energy Fuels, 18, 995–1000, https://doi.org/10.1021/ef049970o, 2004.

Mastalerz, M., Schimmelmann, A., Lis, G. P., Drobniak, A., and Stankiewicz, A.: Influence of maceral composition on geochemical characteristics of immature shale kerogen: Insight from density fraction analysis, Int. J. Coal Geol., 103, 60–69, https://doi.org/10.1016/j.coal.2012.07.011, 2012.

Monger, T. G.: The impact of oil aromaticity on carbon dioxide flooding, SPE symp. enhance. oil recov., 371–381, https://www.osti.gov/biblio/6869910.1984.12708 (last access: 4 November 2023), 1984.

Olukcu, N., Yanik, J., Saglam, M., Yuksel, M., and Karaduman, M.: Solvent effect on the extraction of Beypazari oil shale, Energy Fuels, 13, 895–902, https://doi.org/10.1021/ef9802678, 1999.

Overland, I.: Future Petroleum Geopolitics: Consequences of Climate Policy and Unconventional Oil and Gas, Handb. Clean Energy Syst., 1–29, https://doi.org/10.1002/9781118991978.hces203, 2015.

Peters, K. E.: Guidelines for Evaluating Petroleum Source Rock Using Programmed Pyrolysis, Am. Assoc. Petrol. Geol. Bull., 70, 318–329, https://doi.org/10.1306/94885688-1704-11d7-8645000102c1865d, 1986.

Qi, Y., Ju, Y., Cai, J., Gao, Y., Zhu, H., Hunag, C., Wu, J., Meng, S., and Chen, W.: The effects of solvent extraction on nanoporosity of marine-continental coal and mudstone, Fuel, 235, 72–84, https://doi.org/10.1016/j.fuel.2018.07.083, 2019.

Qiu, X., Liu, C., Mao, G., Deng, Y., Wang, F., and Wang, J.: Late Triassic tuff intervals in the Ordos basin, Central China: Their depositional, petrographic, geochemical characteristics and regional implications, J. Asian Earth Sci., 80, 148–160, https://doi.org/10.1016/j.jseaes.2013.11.004, 2014.

Schuler, B., Meyer, G., Peña, D., Mullins, O. C., and Gross, L.: Unraveling the Molecular Structures of Asphaltenes by Atomic Force Microscopy, J. Am. Chem. Soc., 137, 9870–9876, https://doi.org/10.1021/jacs.5b04056, 2015.

Schuler, B., Fatayer, S., Meyer, G., Rogel, E., Moir, M., Zhang, Y., Harper, M. R., Pomerantz, A. E., Bake, K. D., Witt, M., Peña, D., Kushnerick, J. D., Mullins, O. C., Ovalles, C., Van Den Berg, F. G. A., and Gross, L.: Heavy Oil Based Mixtures of Different Origins and Treatments Studied by Atomic Force Microscopy, Energy Fuels, 31, 6856–6861, https://doi.org/10.1021/acs.energyfuels.7b00805, 2017.

Shaohui, G., Shuyuan, L., and Kuangzong, Q.: CS2/NMP extraction of immature source rock concentrates, Org. Geochem., 31, 1783–1795, https://doi.org/10.1016/S0146-6380(00)00126-1, 2000.

SY/T 5735-1995: The Oil and Gas Industry Standards of the People's Repub-lic of China, Geochemical evaluation method of continental hydrocarbon source rocks, https://max.book118.com/html/2019/0831/5032240204002122.shtm (last access: 3 November 2023), 1995.

Tong, J., Han, X., Wang, S., and Jiang, X.: Evaluation of structural characteristics of huadian oil shale kerogen using direct techniques (Solid-state ^{13}C NMR, XPS, FT-IR, and XRD), Energy Fuels, 25, 4006–4013, https://doi.org/10.1021/ef200738p, 2011.

Toolan, D. T. W., Isakova, A., Hodgkinson, R., Reeves-Mclaren, N., Hammond, O. S., Edler, K. J., Briscoe, W. H., Arnold, T., Gough, T., Topham, P. D., and Howse, J. R.: Insights into the influence of solvent polarity on the crystallization of poly(ethylene oxide) spin-coated thin films via in situ grazing incidence wide-angle X-ray scattering, Macromolecules, 49, 4579–4586, https://doi.org/10.1021/acs.macromol.6b00312, 2016.

Wang, Q., Ye, J. Bin, Yang, H. Y., and Liu, Q.: Chemical Composition and Structural Characteristics of Oil Shales and Their Kerogens Using Fourier Transform Infrared (FTIR) Spectroscopy and Solid-State ^{13}C Nuclear Magnetic Resonance (NMR), Energy Fuels, 30, 6271–6280, https://doi.org/10.1021/acs.energyfuels.6b00770, 2016.

Wang, Q., Hou, Y., Wu, W., Niu, M., Ren, S., and Liu, Z.: The relationship between the humic degree of oil shale kerogens and their structural characteristics, Fuel, 209, 35–42, https://doi.org/10.1016/j.fuel.2017.07.077, 2017.

Wang, Y., Liu, L., and Cheng, H.: Pore structure of Triassic Yanchang mudstone, Ordos Basin: Insights into the impact of solvent extraction on porosity in lacustrine mudstone within the oil window, J. Petrol. Sci. Eng., 195, 107944, https://doi.org/10.1016/j.petrol.2020.107944, 2020.

Wei, L., Mastalerz, M., Schimmelmann, A., and Chen, Y.: Influence of Soxhlet-extractable bitumen and oil on porosity in thermally maturing organic-rich shales, Int. J. Coal Geol., 132, 38–50, https://doi.org/10.1016/j.coal.2014.08.003, 2014.

Yang, H., Zhou, P., Xiong, C., Yu, S., and Li, J.: Integrity Evaluation of Cement Ring during Fracturing and Flowback of Horizontal Well in Jimsar Shale Oil, Lithosphere, 4, 6519109, https://doi.org/10.2113/2021/6519109, 2021.

Yang, S., Qiao, H., Cheng, B., and Hu, Q.: Solvent extraction efficiency of an Eocene-aged organic-rich lacustrine shale, Mar. Petrol. Geol., 126, 104941, https://doi.org/10.1016/j.marpetgeo.2021.104941, 2021.

Yang, Z., Zou, C. N., Wu, S. T., Lin, S. H., Pan, S. Q., Niu, X. B., Men, G. T., Tang, Z. X., Li, G. H., Zhao, J. H., and Jia, X. Y.: Formation, distribution and resource potential of the "sweet areas (sections)" of continental shale oil in China, Mar. Petrol. Geol., 102, 48–60, https://doi.org/10.1016/j.marpetgeo.2018.11.049, 2019.

Zhao, X., Liu, Z., Lu, Z., Shi, L., and Liu, Q.: A study on average molecular structure of eight oil shale organic matters and radical information during pyrolysis, Fuel, 219, 399–405, https://doi.org/10.1016/j.fuel.2018.01.046, 2018.

Zhou, L., Zhao, X., Chai, G., Jiang, W., Pu, X., Wang, X., Han, W., Guan, Q., Feng, J., and Liu, X.: Key exploration & development technologies and engineering practice of continental shale oil: A case study of Member 2 of Paleogene Kongdian Formation in Cangdong Sag, Bohai Bay Basin, East China, Petrol. Explor. Dev., 47, 1138–1146, https://doi.org/10.1016/S1876-3804(20)60124-0, 2020.

Zhou, S., Yan, D., Tang, J., and Pan, Z.: Abrupt change of pore system in lacustrine shales at oil- and gas-maturity during catagenesis, Int. J. Coal Geol., 228, 103557, https://doi.org/10.1016/j.coal.2020.103557, 2020.